Published by Institute of Physics Publishing for SISSA

Received: *February 27, 2008*
Revised: *May 9, 2008*
Accepted: *May 30, 2008*
Published: *June 10, 2008*

Inclusive transverse mass analysis for squark and gluino mass determination

Mihoko M. Nojiri

Theory Group, KEK and the Graduate University for Advanced Study (SOKENDAI), Oho 1-1, Tsukuba, Ibaraki, 305-0801, Japan, and
Institute for the Physics and Mathematics of the Universe (IPMU), University of Tokyo, 5-1-5 Kashiwa-noHa, Kashiwa, Chiba, 277-8568, Japan
E-mail: nojiri@post.kek.jp

Yasuhiro Shimizu

Theory Group, KEK, Oho 1-1, Tsukuba, Ibaraki, 305-0801, Japan
E-mail: yshimizu@post.kek.jp

Shogo Okada and Kiyotomo Kawagoe

Department of Physics, Kobe University, Kobe 657-8501, Japan
E-mail: shogo.okada@stu.kobe-u.ac.jp, kawagoe@kobe-u.ac.jp

Abstract: We propose an inclusive analysis of a stransverse mass (m_{T2}) using a hemisphere method. The hemisphere method is an algorithm to group collinear and high p_T particles and jets, assuming that there are two of such groups in a event. An inclusive m_{T2} is defined as a function of an unknown LSP mass, two hemisphere momenta, and missing transverse momentum. Kinematical end points of m_{T2} distributions provide information on sparticle masses. We perform a Monte Carlo simulation to study the inclusive m_{T2} distribution at the LHC. We show that the end point of the inclusive m_{T2} distribution as a function of a test LSP mass has a kink-like structure around the true LSP mass. We find that the inclusive analysis is useful for obtaining information on the heaviest of squark/gluino.

Keywords: Supersymmetric Standard Model, Supersymmetry Phenomenology.

JHEP06(2008)035

Contents

JHEP06(2008)035

1. Introduction

While the particle interactions at low energy are described correctly by the standard model (SM), the mechanism of electroweak symmetry breaking by the Higgs boson suffers from the fine turning problem. In addition, the SM is not successful for describing the dark matter in our Universe.

We expect to obtain information on the physics beyond the SM from the ATLAS and the CMS experiments at the LHC, which is scheduled to start in 2008. Among various proposals, the phenomenology of models with quark and gauge partners with a multiplicatively conserved parity, such as supersymmetric models with conserved R parity [1 – 3], Little Higgs models with T parity [4, 5] and universal extra dimension models [6], get much attention. In the supersymmetric models, quark and gluon partners (squark and gluino) are pair-produced at the LHC, and subsequently decay into SM particles and lightest supersymmetric particles (LSPs). Signatures at the LHC will be high p_T jets and leptons and significant missing transverse momentum which arises from the LSPs escaping detection. By the end of the LHC experiment, squarks and gluinos in the minimal supergravity model will be searched for up to $\sim 2.5\,\mathrm{TeV}$ [7, 8].

Interests in new physics go beyond the discovery. Many studies have been carried out to find out possible clues to study the "nature of the new physics," such as masses, spins and interactions of new particles. Progress has been made especially in exclusive channels. End points of invariant mass distributions constrain sparticle masses and for some cases nearly all sparticle masses can be measured. The end point study is extremely successful for leptonic channels [7 – 12].

The other important variables are inclusive transverse masses. The peak of the effective mass distribution, which is the sum of the transverse momenta of jets, leptons and E_T^{miss},

is sensitive to the sum of the sparticle masses directly produced by pp collisions. The quantity is inclusive and would be useful in the early stage of the LHC experiment. A more sophisticated quantity is the m_{T2} variable [13, 14]. This can be calculated from two visible objects, the missing momentum of a event, and a test LSP mass. Without knowledge of the LSP mass, the m_{T2} end point is regarded as a function of a test LSP mass. Recently, the variable has attracted much attention because this function has a kink at the correct LSP mass when a squark/gluino undergoes three body decays. Several exercises have been carried out, especially for gluino-gluino production, but also for several other production and decay channels without specifying selection processes [15 – 18].

In this paper we propose an inclusive study of the m_{T2} variable using a hemisphere method. Namely we group jets into two "visible objects" and calculate the m_{T2} variable based on them. We take the hemisphere method as a grouping algorithm [19, 20]. The motivation for using the hemisphere algorithm is to collect cascade decay products from a squark or a gluino, so that the m_{T2} end point provides information on squark and gluino masses without going into an exclusive analysis.

The inclusive m_{T2} variable is sensitive to $\max(m_{\tilde{g}}, m_{\tilde{q}})$ as m_{T2} is defined from the larger of the transverse masses of the two visible objects for test LSP momenta consistent with $p_T^{\rm miss}$. Not surprisingly, the probability of reconstructing the correct decay products is rather low and the end point is smeared. However, event-wise response of the m_{T2} variable to the test LSP mass mentioned in refs. [15 – 18] would be useful in ensuring that the true end point was found.

In this paper, we also compare the mixed modulus anomaly mediation (MMAM) model to the minimal supergravity (mSUGRA) model. The MMAM model predicts a degenerate mass spectrum in some parameter regions of the model. In such a degenerate mass spectrum, the available p_T's of the daughter particles are small although the sparticles are heavy. To compare the two models, we take sample spectra from each model in which the $M_{\rm eff}$ distributions are very similar and the total cross sections are the same. However, the LSP mass in the MMAM model is significantly heavier in the mSUGRA while the squark in the mSUGRA model is significantly heavier that in the MMAM model. Without the inclusive m_{T2} analysis, these two points may be indistinguishable.

At the MMAM sample point, we find that the end point of m_{T2} is determined by the gluino mass. The kink structure appears at the true LSP mass and the gluino and LSP masses are determined simultaneously. At the mSUGRA sample point, we find that the end point of m_{T2} is determined by the squark mass. We also show good linearity between squark masses and end points of m_{T2} for several mSUGRA sample points with $m_{\tilde{q}} > m_{\tilde{g}}$. However, we cannot see a kink structure, and so it is difficult to determine the LSP mass. For both cases, we can obtain information on sparticle masses.

This paper is organized as follows. In section 2 we review the m_{T2} variable and the kink structure appearing in the end point as a function of a test LSP mass. In section 3 we describe the inclusive m_{T2} and perform Monte Carlo simulations to study distributions. section 4 is devoted to the conclusion.

JHEP06(2008)035

2. The stransverse mass (m_{T2})

In hadron collisions, squarks and gluinos are copiously produced in pairs and these SUSY particles decay subsequently into final states including jets, leptons, and two LSPs. We assume that the LSP is the lightest neutralino. With conserved R-parity, the LSP is neutral and stable, and escapes detection. There are two LSPs in each event and while one cannot measure each LSP momentum experimentally, the total transverse momentum can be measured. The stransverse mass m_{T2} is defined as follows:

$$m_{T2}^2(m_\chi) \equiv \min_{\mathbf{p}_{T1}^{\rm miss}+\mathbf{p}_{T2}^{\rm miss}=\mathbf{p}_T^{\rm miss}} \left[\max\left\{m_T^2(\mathbf{p}_{T1}^{\rm vis},\mathbf{p}_{T1}^{\rm miss}), m_T^2(\mathbf{p}_{T2}^{\rm vis},\mathbf{p}_{T2}^{\rm miss})\right\}\right], \tag{2.1}$$

where $\mathbf{p}_{Ti}^{\rm vis}$ is the transverse momentum of the "visible objects" from a squark/gluino decay, which is defined as the sum of visible particle momenta. The minimization is taken with respected to the unknown LSP momenta $\mathbf{p}_{T1}^{\rm miss}$, $\mathbf{p}_{T2}^{\rm miss}$ under the constraint $\mathbf{p}_{T1}^{\rm miss}+\mathbf{p}_{T2}^{\rm miss}=\mathbf{p}_T^{\rm miss}$, where $\mathbf{p}_T^{\rm miss}$ is the total missing transverse momentum. The transverse mass, m_T^2, is defined as

$$m_T^2\left(\mathbf{p}_{Ti}^{\rm vis},\mathbf{p}_{Ti}^{\rm miss}\right) = (m_i^{\rm vis})^2 + m_\chi^2 + 2\left(E_{Ti}^{\rm vis}E_{Ti}^{\rm miss} - \mathbf{p}_{Ti}^{\rm vis}\cdot\mathbf{p}_{Ti}^{\rm miss}\right), \tag{2.2}$$

where $E_{Ti}=\sqrt{p_{Ti}^2+m_\chi^2}$ and $m_i^{\rm vis}$ is the total visible invariant mass of the "visible object." It should be noted that the true LSP mass ($m_{\chi_1^0}$) is unlikely to be known in advance, so m_{T2} is regarded as a function of a test LSP mass (m_χ).

The m_{T2} variable is smaller than parent gluino/squark masses if the test LSP mass is set equal to the true value.

$$m_{T2}(m_{\chi_1^0}) \le \max(m_{\tilde q}, m_{\tilde g}). \tag{2.3}$$

From the upper end point of the m_{T2} ($m_{T2}^{\rm max}$), one can obtain information on the mass of the parent particle. Without knowledge of the true LSP mass, $m_{T2}^{\rm max}$ provides a one-dimensional constraint between masses of squark/gluino and the LSP.

Recently, it was pointed out that the $m_{T2}^{\rm max}(m_\chi)$ function has a kink structure at which m_χ is the true LSP mass unless squark/gluino decays directly into the LSP through a two body decay. An analytic expression for $m_{T2}^{\rm max}$ is derived in refs. [17, 18]. If one considers events in which squarks or gluinos are produced in pairs with a vanishing total transverse momentum, $m_{T2}^{\rm max}(m_\chi)$ is given as follows.

$$m_{T2}^{\rm max}(m_\chi) = \begin{cases} \mathcal{F}_<^{\rm max}(m_\chi) & \text{for } m_\chi < m_{\chi_1^0} \\ \mathcal{F}_>^{\rm max}(m_\chi) & \text{for } m_\chi > m_{\chi_1^0}, \end{cases} \tag{2.4}$$

where

$$\begin{aligned} \mathcal{F}_<^{\rm max}(m_\chi) &= \mathcal{F}(m_1^{\rm vis}=m_{\rm min}^{\rm vis}, m_2^{\rm vis}=m_{\rm min}^{\rm vis}, \theta=0, m_\chi), \\ \mathcal{F}_>^{\rm max}(m_\chi) &= \mathcal{F}(m_1^{\rm vis}=m_{\rm max}^{\rm vis}, m_2^{\rm vis}=m_{\rm max}^{\rm vis}, \theta=0, m_\chi). \end{aligned} \tag{2.5}$$

Here the function $\mathcal{F}$ is given in ref. [18] and $m_i^{\rm vis}$ is kinematically bounded as follows,

$$m_{\rm min}^{\rm vis} \le m_i^{\rm vis} \le m_{\rm max}^{\rm vis}. \tag{2.6}$$

Notice that events at the end point satisfy $m_i^{\rm vis} = m_{\rm min}^{\rm vis}$ for $m_\chi < m_{\chi_1^0}$ while $m_i^{\rm vis} = m_{\rm max}^{\rm vis}$ for $m_\chi > m_{\chi_1^0}$. A kink structure appears in $m_{T2}^{\rm max}(m_\chi)$ since the functional form of $m_{T2}^{\rm max}(m_\chi)$ changes at $m_\chi = m_{\chi_1^0}$. In ref. [17], it is shown that the kink structure appears even if the pair-produced squark and gluino have a non-vanishing transverse momentum. If one can identify the position of the kink from LHC experiments, masses of squark/gluino and the LSP can be determined simultaneously. In ref. [18], it is demonstrated that masses of squark/gluino and the LSP can be determined using exclusive decay channels by performing Monte Carlo simulations for model points. In particular, for the case that a gluino decay $\tilde{g} \to qq\chi_1^0$ occurs through an off-shell squark exchange diagram, $m_{T2}^{\rm max}$ from gluino pair-production has a very sharp kink structure and the masses are determined precisely.

3. The inclusive m_{T2} analysis

3.1 The hemisphere analysis and the inclusive m_{T2} variable

In this section we argue that the kink method discussed in section 2 should be extended to an inclusive analysis. In exclusive analyses, one needs to specify a cascade decay chain. The branching ratio of a cascade decay chain would depend on model parameters. By comparison, inclusive distributions are rather insensitive to branching ratios. Therefore, if an inclusive quantity can be defined, it may be useful for determining squark and gluino masses in the early stage of the LHC experiment. A disadvantage of the inclusive approaches may be that all the production and decay modes contribute to the distribution, introducing unknown systematic errors.

To define an inclusive m_{T2} distribution, we group the particles in an event into two "visible objects." For this purpose, we adopt the hemisphere method in refs. [19, 20]. For each event, two hemispheres are defined and high p_T jets, leptons, and photons are assigned into one of the hemispheres as follows;

1. Each hemisphere is defined by an axis $p_i^{\rm vis}(i = 1, 2)$, which is the sum of the momenta of all high p_T objects belonging to the hemisphere i. We require $p_T > 50\,\text{GeV}$ for jets to reduce QCD backgrounds.

2. A high p_T object k belonging to a hemisphere i satisfies the following conditions:

$$d(p_k, p_i^{\rm vis}) < d(p_k, p_j^{\rm vis}), \tag{3.1}$$

where the function d is defined by

$$d(p_k, p_i^{\rm vis}) = (E_i - |p_i^{\rm vis}| \cos\theta_{ik}) \frac{E_i}{(E_i + E_k)^2}. \tag{3.2}$$

Here θ_{ik} is the angle between $p_i^{\rm vis}$ and p_k.

To find the $p_i^{\rm vis}$ axes, we adopted the algorithm discussed in refs. [19, 20]. Once $p_i^{\rm vis}$'s are determined, one can calculate m_{T2} by using eq. (2.1).

The inclusive m_{T2} may be compared with m_{TGen} [21]. The m_{TGen} variable is the minimum of the m_{T2} variable for all possible choices of two subsets of particles α and β.

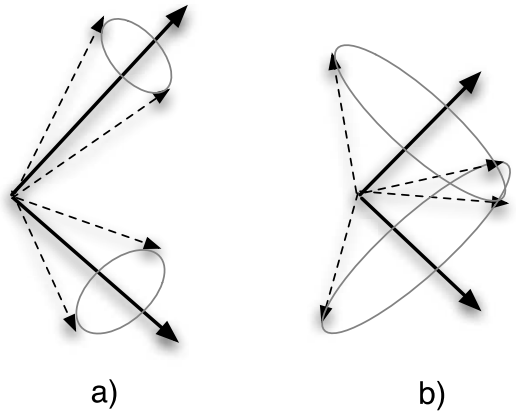

Figure 1: Kinematical configurations for (a) $m^{\rm vis} \sim m^{\rm vis}_{\rm min}$ and (b) $m^{\rm vis} \sim m^{\rm vis}_{\rm max}$. When $m^{\rm vis}$ is large, jets in the hemisphere are less collinear, and the hemisphere analysis likely misgroups the particles.

The end point of m_{TGen} should be bounded from above by the parent mass, if the initial state radiation can be ignored. The correct choice of subsets α and β leads to the heaviest sparticle mass as the end point.

The approach is useful if the algorithm described above groups high p_T jets from a cascade decay. This should be the case when the decay products are collinear, i.e. when $d(p_k, p_i^{vis})$ among the decay products is small. The visible hemisphere mass should be small compared with the $p_T^{\rm vis}$ in this case. Conversely, if $m^{\rm vis}$ is large compared with $p_T^{\rm vis}$, the probability of misgrouping jets is large, see figure 1.

3.2 Model points

To perform Monte Carlo analyses, we choose two sample points, A and B. The point A corresponds to the MMAM model [22 – 25]. In the MMAM model, the mass spectrum is parametrized by the modular weights for matter fields n_i, the gravitino mass ($m_{3/2}$) and $R \equiv m_{3/2}\langle (T+T^*)/F_T \rangle$ where T and F_T are a modulus field and its F-component, respectively. In general, the MMAM model predicts a degenerate SUSY spectrum compared with the mSUGRA model. If $\alpha = R/\ln(M_{\rm Pl}/m_{3/2})$ is large, the SUSY spectrum becomes more degenerate. In this analysis, we choose the point studied in ref. [26]: $n_i = 0(1)$ for squarks and sleptons (Higgs boson), $R = 20$, $\tan\beta = 10$, and the gravitino mass is such that $M_3 = 650\,\text{GeV}$ at the GUT scale, which corresponds to $\alpha = 0.62$. The point B corresponds to mSUGRA with $m_0 = 1475\,\text{GeV}$, $m_{1/2} = 561\,\text{GeV}$, $A = 0$ and $\tan\beta = 10$.

The mass spectrum of SUSY particles is calculated using ISAJET [27] for each sample point. In table 1, the relevant SUSY masses are listed. At point B, $m_{\tilde{q}} > m_{\tilde{g}}$ and the gluino undergoes a three-body decay through off-shell squark diagrams. The total production cross section of sparticles at the LHC is $\sigma = 0.13$ pb for both points. The cross section of squark-gluino co-production is larger than those of the squark-squark and gluino-gluino production for both points.

JHEP06(2008)035

	A: MMAM	B: mSUGRA
	$n_i = 0$, $R = 20$, $M_3(\mathrm{GUT}) = 650$	$m_0 = 1475$, $m_{1/2} = 561.2$, $A = 0$, $\tan\beta = 10$
$\tilde{g}$	1491	1359
$\tilde{u}_L$	1473	1852
$\tilde{u}_R$	1431	1831
$\tilde{d}_R$	1415	1830
$\tilde{\chi}_1^0$	487	237

Table 1: The relevant SUSY mass parameters at points A and B. All the mass parameters are given in GeV.

The point B is chosen so that the $M_{\rm eff}$ distribution of the one-lepton mode is very similar to that for point A,[1] where $M_{\rm eff}$ is defined from the sum of p_T's of the first four hardest jets, a lepton and the missing transverse momentum as follows,

$$M_{\rm eff} = \sum_{i=1}^{4} p_{Ti} + p_{Tl} + E_T^{\rm miss}. \tag{3.3}$$

For the Monte Carlo analysis, we generate 5×10^4 SUSY events using HERWIG 6.5 [28] for each sample point.[2] To estimate event distributions measured by the LHC detector, we use AcerDET [29]. This code provides a simple detector simulation, jet reconstruction, and particle identification at the LHC.

In figure 2(a), $M_{\rm eff}$ distributions are shown for the one-lepton channel. Here we require the following cuts.

1. $n_{\rm jet}(p_T > 100\ \mathrm{GeV}) \equiv n_{100} \geq 1$ and $n_{\rm jet}(p_T > 50\ \mathrm{GeV}) \equiv n_{50} \geq 4$ within $|\eta| < 3$.
2. $E_T^{\rm miss} > 0.2 M_{\rm eff}$ and $E_T^{\rm miss} > 100\,\mathrm{GeV}$ and $S_T > 0.2$. Here S_T is the transverse sphericity.
3. Only one isolated lepton with $p_T > 20\,\mathrm{GeV}$.

The solid (dashed) histogram is the distribution for point A (B) and the $M_{\rm eff}$ distributions roughly agree with each other.

Although there is not much difference in the $M_{\rm eff}$ distribution defined in eq. (3.3), there are more high p_T jets on average at point B compared with point A. This is because the squark-gluino co-production is dominant, and a squark decaying into a gluino leads an additional high pt jet in the events. If one sums all jets with p_T >50 GeV, then the distribution for point B is significantly harder than that of point A. In figure 2(b), this is plotted for the one-lepton channel and the difference between the two points is more

[1] We have considered the one-lepton mode since the the SM background for this mode is rather small, which is important for discovery of SUSY particles. For the zero lepton channel, the peak position of the $m_{\rm eff}$ distributions roughly agree with each other, but the distribution is harder for Point B.

[2] We have generated 5 $\times 10^4$ to avoid large statistical fluctuations in various distributions.

JHEP06(2008)035

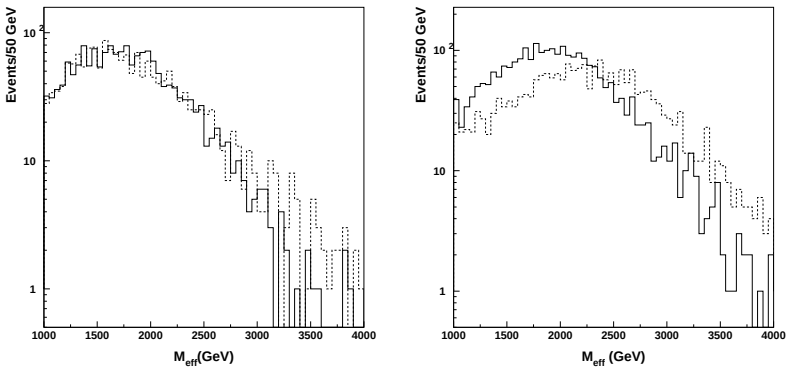

Figure 2: (a) $M_{\rm eff}$ distributions for the one-lepton channel. The solid (dashed) histogram is for point A (B). (b) $M_{\rm eff}$ distributions for the one-lepton channel as in (a) but summing up all jets with $p_T > 50\,\text{GeV}$. The solid (dashed) histogram is for point A (B).

prominent. This shows that there are more than four hard partons on average for Point B, but it is not clear what kind of quantitative conclusion can be drawn from that. We will see in the next subsections that the inclusive m_{T2} analysis gives us a more quantitative measure of the difference between the two points.

3.3 Monte Carlo analysis: point A (MMAM)

First, let us consider point A. We require the following cuts to select the events.

1. $n_{100} \geq 2$ and $n_{50} \geq 4$ within $|\eta| < 3$.

2. The effective mass of the event must satisfy $M_{\rm eff} > 1200\,\text{GeV}$.

3. At least two jets in each hemisphere.

4. $E_T^{\rm miss} > 0.2 M_{\rm eff}$ and $E_T^{\rm miss} > 100\,\text{GeV}$.

5. No isolated lepton with $p_T > 20\,\text{GeV}$.

Here we take no lepton events since the m_{T2} variable assumes that there is no source of missing momenta except for the LSPs while hard leptons may be associated with neutrinos. With these cuts, the SM backgrounds are expected to be small. We do not consider the SM backgrounds in this simulation and the distribution of the SM backgrounds in the m_{T2} analysis will be discussed elsewhere.

To check how well the hemisphere method works, let us consider the following ratio:

$$R(m_\chi) \equiv \frac{m_{T2}(m_\chi) - m_{T2}^{(p)}(m_\chi)}{m_{T2}^{(p)}(m_\chi)}, \tag{3.4}$$

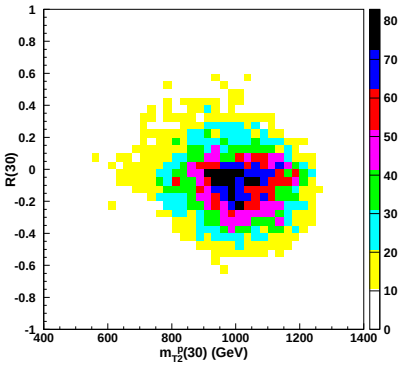

Figure 3: The two-dimensional distribution in the $m_{T2}^{(p)}$-R plane for point A. The test LSP mass is assumed to be $m_\chi = 30\,\mathrm{GeV}$.

where the parton level $m_{T2}^{(p)}$ is defined so that each visible momentum is the difference of an initially produced sparticle and the daughter LSP momentum, and E_T^{miss} is the missing energy provided by AcerDET after smearing.[3]

In figure 3, a two-dimensional distribution in the $m_{T2}^{(p)}$-R plane is shown for $m_\chi = 30\,\mathrm{GeV}$. The peak of the distribution appears around $R \sim 0$, but deviation from $R = 0$ can be large. The reconstructed m_{T2} tends to be smaller than $m_{T2}^{(p)}$. The main sources of the deviation is misgrouping of visible objects under the hemisphere method, and also neutrinos and jets with $p_T < 50\,\mathrm{GeV}$ which are not included in the hemisphere definition.

Let us consider m_{T2} distributions for $m_\chi < m_{\chi_1^0}$. In figure 4(a), the $m_{T2}^{(p)}$ distribution is shown for $m_\chi = 30\,\mathrm{GeV}$. There is an end point at $m_{T2}^{(p)} \simeq 1250\,\mathrm{GeV}$. In figure 4(b), the reconstructed m_{T2} distribution is shown for $m_\chi = 30\,\mathrm{GeV}$. Compared with the $m_{T2}^{(p)}$ distribution, there is a long tail due to misgrouping in the hemisphere method, although there is some structure at $m_{T2} \sim 1350\,\mathrm{GeV}$.

Let us examine events around the end point region in detail. Figure 5(a) shows a $\max(m_1^{\mathrm{vis}}, m_2^{\mathrm{vis}})$ distribution for $m_{T2}(30) > 1000\,\mathrm{GeV}$. As discussed in section 2, the true end point events satisfy $m_i^{\mathrm{vis}} = m_{\mathrm{min}}^{\mathrm{vis}}$ and events with large $\max(m_1^{\mathrm{vis}}, m_2^{\mathrm{vis}})$ must be fake events. To reduce them, the m_{T2} distribution for $\max(m_1^{\mathrm{vis}}, m_2^{\mathrm{vis}}) < 400\,\mathrm{GeV}$ is plotted in figure 5(b). With the cut on the hemisphere mass, the long tail of m_{T2} disappears and one can see a rather clear end point at $m_{T2} \sim 1350\,\mathrm{GeV}$.

Next, let us consider m_{T2} distributions for $m_\chi > m_{\chi_1^0}$. In figure 6(a), the $m_{T2}^{(p)} - m_\chi$ distribution is plotted for $m_\chi = 900\,\mathrm{GeV}$. There is an end point at $m_{T2}^{(p)} \sim 1900\,\mathrm{GeV}$. In figure 6(b), the reconstructed $m_{T2} - m_\chi$ distribution is plotted for $m_\chi = 900\,\mathrm{GeV}$. The distribution has a long tail. The end point is less clear compared with figure 4 and the fitted end point is $\sim 2000\,\mathrm{GeV}$.

[3] Alternatively one can choose that E_T^{miss} is the sum of the LSP momenta. However, these two choices give similar m_{T2} distributions. Note that the sum of the transverse momenta of produced sparticles is not zero due to initial state radiation. This leads to smearing for the $m_{T2}^{(p)}$ distribution.

JHEP06(2008)035

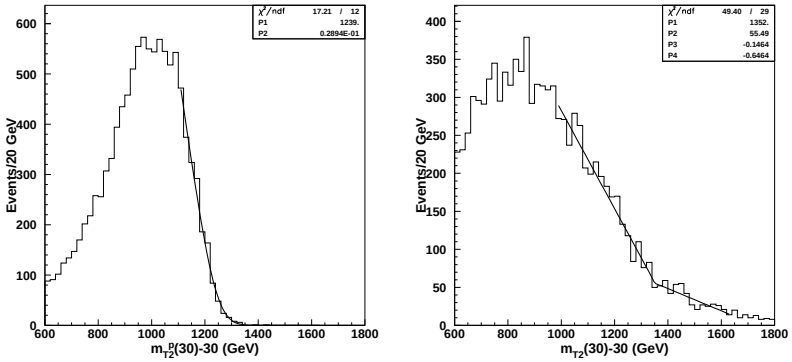

Figure 4: (a) The $m_{T2} - m_\chi$ distribution at parton level for $m_\chi = 30\,\mathrm{GeV}$. (b) The reconstructed $m_{T2} - m_\chi$ distribution for $m_\chi = 30\,\mathrm{GeV}$. Fitting functions for the end points are also shown, see text.

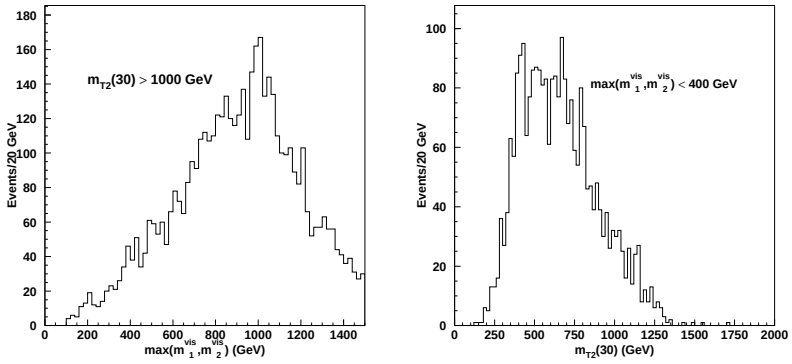

Figure 5: (a) The distribution of $\max(m_1^{\mathrm{vis}}, m_2^{\mathrm{vis}})$ for $m_{T2}(30) > 1000\,\mathrm{GeV}$. (b) The $m_{T2}(30)$ distribution for $\max(m_1^{\mathrm{vis}}, m_2^{\mathrm{vis}}) < 400\,\mathrm{GeV}$.

To find the end points of the m_{T2} distributions, we also show the fit to the distribution in figures 4 and 6. We fit the reconstructed m_{T2} distribution with a linear function which changes slope at some m_χ. For comparison, we also show a fit of $m_{T2}^{(p)}$. For this we use a Gaussian smeared fitting function from ref. [11]. We find that $\chi^2/\mathrm{n.d.f's} \gg 1$, therefore our fits should be regarded as crude estimations. In addition, the end point for $m_\chi = 900\,\mathrm{GeV}$ depends on the bins used for the fit. Note that the end point for $m_\chi > m_{\tilde{\chi}_1^0}$ is realized for events with $m^{\mathrm{vis}} \sim m_{\mathrm{max}}^{\mathrm{vis}}$, while the efficiency for assigning the particles to a correct hemisphere should be low in such case, see figure 1. In the previous section, we noted that events near m_{T2}^{max} are dominated by events with $m^{\mathrm{vis}} \sim m_{\mathrm{min}}^{\mathrm{vis}}(m_{\mathrm{max}}^{\mathrm{vis}})$ for $m_\chi < (>)\, m_{\chi_1^0}$. This means that determination of m_{T2}^{max} for $m_\chi < m_{\chi_1^0}$ is more reliable than that for $m_\chi > m_{\chi_1^0}$.

As discussed in section 2, a kink structure appears in m_{T2}^{max} since the functional form of

JHEP06(2008)035

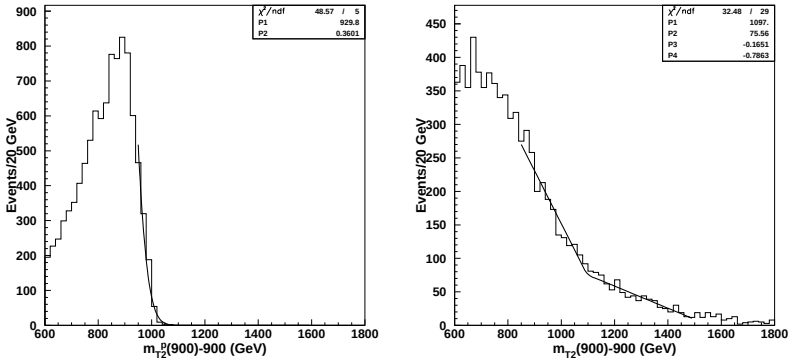

Figure 6: (a) The $m_{T2} - m_\chi$ distribution at parton level for $m_\chi = 900\,\text{GeV}$. (b) The reconstructed $m_{T2} - m_\chi$ distribution for $m_\chi = 900\,\text{GeV}$. Fitting functions for the end points are also shown, see text.

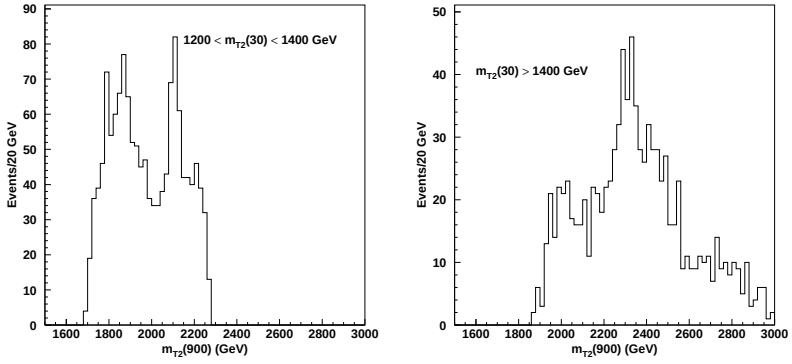

Figure 7: (a) The $m_{T2}(900)$ distribution for $1200\,\text{GeV} < m_{T2}(30) < 1400\,\text{GeV}$ (left). (b) The $m_{T2}(900)$ distribution for the fake events $m_{T2}(30) > 1400\,\text{GeV}$ (right).

$m_{T2}^{\max}(m_\chi)$ changes at $m_\chi = m_{\chi_1^0}$. End point events for $m_\chi < m_{\chi_1^0}$ are different from those for $m_\chi > m_{\chi_1^0}$ and these end point events are interchanged at $m_\chi = m_{\chi_1^0}$. To confirm this, let us consider how events near the end point of $m_{T2}(30)$ behaves when m_χ is large. In figure 7(a), a $m_{T2}(900)$ distribution is plotted for $1200\,\text{GeV} < m_{T2}(30) < 1400\,\text{GeV}$. There are two peaks in the distribution. The lower peak is consistent with correctly reconstructed events because $m_{T2}(900)$ is smaller than the fitted end point for $m_{T2}(900) \sim 2000\,\text{GeV}$. In figure 7(b), the $m_{T2}(900)$ distribution is plotted for events above the true end point for $m_{T2}(30)$, $m_{T2}(30) > 1400\,\text{GeV}$. We find no peak lower than 2000 GeV as expected, because they are fake events for $m_{T2}(30)$. In general, the reconstructed m_{T2} distributions have a long tail and it is unclear whether the fitted end points arise from correctly reconstructed events. The behaviour of the events above and below the end point with respect to a test LSP mass provide confirmation of the correctness of the end point and an event-wise check whether or not the event has been reconstructed correctly.

In figure 8, end points of m_{T2} for various test LSP masses are plotted with solid lines.

JHEP06(2008)035

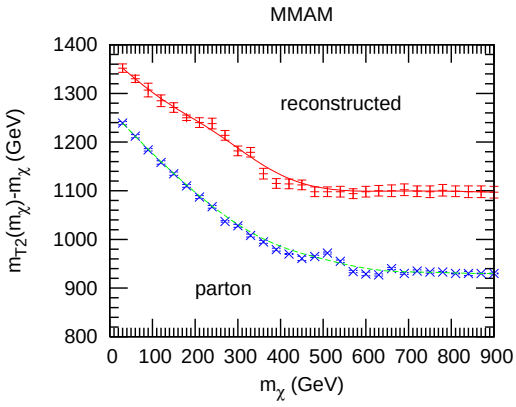

Figure 8: End points of $m_{T2}(m_\chi) - m_\chi$ for various test LSP masses. The solid line is the $m_{T2}^{\max}$ while the dashed line is the parton level $m_{T2}^{(p)\max}$.

The end points of the m_{T2} are larger than $m_{T2}^{(p)}$ by $150 - 200\,\text{GeV}$, and one can see a kink structure around $m_\chi \sim 400\,\text{GeV}$, which is close to the true LSP mass, $m_{\chi_1^0} = 487\,\text{GeV}$. At the kink, the end point value of m_{T2} is $m_{T2}^{\max} \sim 1550\,\text{GeV}$. It should be noted that the inclusive m_{T2} distribution is dominated by the events from squark-gluino co-production since the production cross section is larger than those of gluino-gluino and squark-squark pair production. In such a situation, the end point of m_{T2} distributions is sensitive to $\max(m_{\tilde{g}}, m_{\tilde{q}})$. At point A, the gluino is heavier than the squarks and the end point should be sensitive to the gluino mass, $m_{\tilde{g}} = 1491\,\text{GeV}$. While the end point value is larger than the true gluino mass by about 150 GeV, we think the agreement between m_{T2} and $m_{T2}^{(p)}$ is reasonable given the crudeness of our fit.

In mSUGRA, a bino-like LSP has about 1/6 of the gluino mass. If we take the measured m_{T2} end point at the kink as the gluino mass then the LSP mass assuming mSUGRA is around 270 GeV. The observed kink is clearly above 270 GeV, therefore we can say that the mass spectrum is different from the one of the mSUGRA model.

3.4 Monte Carlo analysis: point B (mSUGRA)

At point B, squarks are much heavier than gluinos and our interest is in measuring the squark mass scale using the inclusive m_{T2} distributions. We require the following cuts to select the events:

1. $n_{100} \geq 2$ and $n_{50} \geq 6$ within $|\eta| < 3$.
2. $M_{\text{eff}} > 1500\,\text{GeV}$.[4]
3. At least two jets in each hemisphere.

[4]We have taken a different M_{eff} cut from the one in Point A in order to consider the squark-gluino production events. In principle a higher M_{eff} cut is better for the hemisphere reconstruction, and the cut is increased because the number of no lepton events for Point B is larger than that of Point A.

JHEP06(2008)035

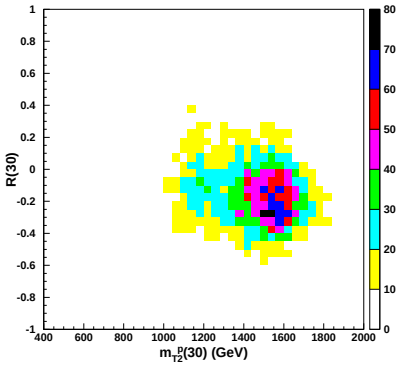

Figure 9: The two-dimensional distribution in m_{T2}-R plane for point B. A test LSP mass of $m_\chi = 30\,\mathrm{GeV}$ is assumed.

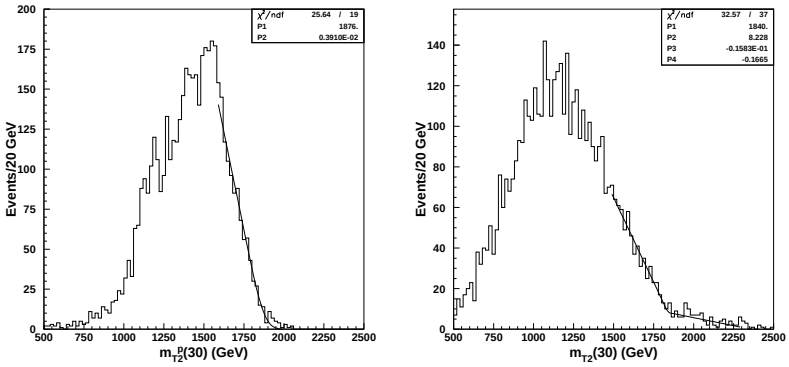

Figure 10: (a) The $m_{T2}^{(p)}$ distribution, (b) The m_{T2} distribution for $m_\chi = 30\,\mathrm{GeV}$.

4. $E_T^{\mathrm{miss}} > 0.2 M_{\mathrm{eff}}$ and $E_T^{\mathrm{miss}} > 100\,\mathrm{GeV}$.

5. No isolated lepton with $p_T > 20\,\mathrm{GeV}$.

In figure 9 a two-dimensional distribution in the $m_{T2}^{(p)}$-R plane is plotted for $m_\chi = 30\,\mathrm{GeV}$. The peak of the distribution appears at $R \sim -0.2$, and the misreconstruction rate is higher than at point A. The low reconstruction efficiency may be understood as follows. At this point $m_{\tilde{q}} \sim 1850\,\mathrm{GeV}$, $m_{\tilde{g}} \sim 1360\,\mathrm{GeV}$ and squark decaying into gluino gives high p_T jets as discussed earlier. When this jet is misidentified to the other hemisphere, the reconstructed m_{T2} may become much lower than the expected $m_{T2}^{(p)}$ value, because the squark is so much heavier than the gluino. It can be as low as of the order of the gluino mass. Note that $(m_{\tilde{q}} - m_{\tilde{g}})/m_{\tilde{q}} \simeq 0.26$, roughly corresponds to the observed shift. Luckily, $m_{T2}^{(p)}$ strongly peaks near the end point, and the reconstructed events still make a visible end point in the m_{T2} distribution.

In figure 10(a), the $m_{T2}^{(p)}$ distribution is plotted for $m_\chi = 30\,\mathrm{GeV}$. There are two peaks in the $m_{T2}^{(p)}$ distribution. The higher peak corresponds to the squark while the lower peak

JHEP06(2008)035

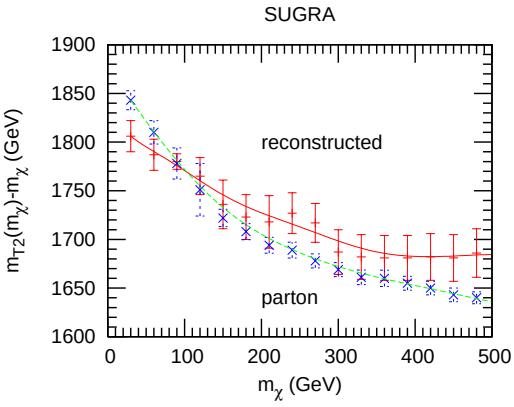

Figure 11: End points of $m_{T2}(m_\chi) - m_\chi$ for various test LSP masses. The solid line is the $m_{T2}^{\max}$ while the dashed line is the parton level $m_{T2}^{(p)\max}$.

corresponds to a gluino. At point B, the squark is much heavier than the gluino, so the end point is determined by the squark decay, $m_{T2}^{(p)} \sim 1850\,\text{GeV}$. In figure 10(b), a m_{T2} distribution is shown for $m_\chi = 30\,\text{GeV}$. The m_{T2} distribution is smeared but one can still see an end point. The end point events are dominated by the events with small m^{vis}. There is again interchange of the events near the end point as we increase the test LSP mass, and we can see the two peak structure in m_{T2} for $m_\chi > m_{\chi_1^0}$ with the events near the end point of m_{T2} for $m_\chi < m_{\chi_1^0}$, similar to figure 7.

In figure 11 end points of m_{T2} for various test LSP masses are plotted with a solid line. The end points are determined as for point A. The end points of the m_{T2} are almost the same as the ones of $m_{T2}^{(p)}$ within errors. One cannot see a clear kink structure around the true LSP mass, $m_{\chi_1^0} = 237\,\text{GeV}$. While it is difficult to determine the neutralino mass from the kink method, the inclusive m_{T2} analysis is useful for obtaining information on the squark mass. To see whether an end point of m_{T2} correctly describes squark masses for $m_{\tilde{q}} > m_{\tilde{g}}$, we show m_{T2} end points for $m_\chi = 30\,\text{GeV}$ at mSUGRA points where the gaugino mass is kept the same as that of point B but the universal scalar mass m_0 is varied. In figure 12 we plot the m_{T2} end point as a function of the squark mass and find very good agreement from 1500 GeV to 1900 GeV.

4. Summary and conclusion

In this paper, we have proposed an inclusive m_{T2} analysis at the LHC in order to obtain information on squark and gluino masses by the hemisphere method. The hemisphere method is an algorithm to group collinear and high p_T particles and jets, assuming that there are two of such groups in an event. At the LHC, squarks and gluinos are produced in pairs and they decay subsequently into SM particles and the LSPs. The algorithm groups the cascade decay products into two visible objects. The m_{T2} is a function of a test LSP mass, m_χ, two visible object masses, m_i^{vis} (hemisphere mass), and the E_T^{miss} of a event. To study the m_{T2} distributions, we perform Monte Carlo simulations for two

JHEP06(2008)035

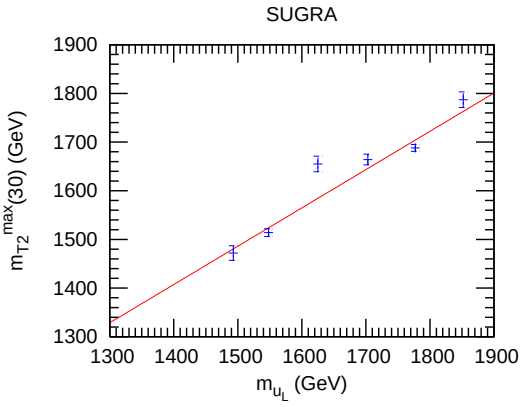

Figure 12: The end point of m_{T2} for $m_\chi = 30$ at several mSUGRA points where gaugino masses are the same as those of point B but m_0 is varied. Here the horizontal axis is the left-handed up-type squark mass.

sample SUSY spectra of the MMAM and mSUGRA models. The cascade decay products from a squark/gluino are grouped into a visible object so that we see the parton level m_{T2} end point. However, the end point of the m_{T2} distribution is sometimes smeared by misidentification of hemispheres, which obscures the end point determination. When we fit m_{T2} distributions near the end points, the end point determination suffers from various systematic uncertainties, such as a choice of the fitting function and the fitting region.

We have examined events near the end point in detail. For $m_\chi < m_{\chi_1^0}$ the end point events have the minimum hemisphere mass, $m_i^{\rm vis} = m_{\rm min}^{\rm vis}$. Fake end point events due to the misgrouping of the hemisphere are reduced if we impose a cut on the hemisphere mass, without disturbing the correct end points. For $m_\chi > m_{\chi_1^0}$, events with a hemisphere mass at maximum $m_i^{\rm vis} = m_{\rm max}^{\rm vis}$ should be near the end point. Therefore, the end point events are interchanged at $m_\chi = m_{\chi_1^0}$ and a kink structure appears in $m_{T2}^{\rm max}$. By checking the test mass behavior of a m_{T2} variable for the events near the end point, we can prove whether events near the end point obtained by the fit to the m_{T2} distribution are correctly reconstructed ones or not. We have shown by doing MC simulations that the true end point events for $m_\chi < m_{\chi_1^0}$ gives an m_{T2} value smaller than the $m_{T2}^{\rm max}$ for $m_\chi \gg m_{\chi_1^0}$, while the fake end point events for $m_\chi < m_{\chi_1^0}$ gives m_{T2} larger than the $m_{T2}^{\rm max}$ for $m_\chi > m_{\chi_1^0}$. From this observation, while there are various uncertainties for the end point determination, we conclude that the inclusive m_{T2} distribution is useful for obtaining information on the masses of gluino/squark and the LSP at the LHC experiment.

For both of the sample points, the main QCD production process for sparticles is squark-gluino co-production, and an end point of the m_{T2} distribution is sensitive to $\max(m_{\tilde{g}}, m_{\tilde{q}})$. At the sample point for the MMAM model, $m_{\tilde{g}} > m_{\tilde{q}}$ and the end point should be determined by $m_{\tilde{g}}$, while it should be determined by $m_{\tilde{q}}$ at the sample point for the mSUGRA model because $m_{\tilde{q}} > m_{\tilde{g}}$. From Monte Carlo analyses, we have found that the end point is indeed determined by $\max(m_{\tilde{g}}, m_{\tilde{q}})$ for both of the sample points. For the

JHEP06(2008)035

MMAM sample point, we have found that there is a kink-like structure in $m_{T2}^{\max}(m_\chi)$ at the true LSP mass and we can determine the gluino and LSP masses simultaneously. For the mSUGRA sample points with $m_{\tilde{q}} > m_{\tilde{g}}$, we find good linearity between $m_{\tilde{q}}$ and $m_{T2}^{\max}$. We have checked that squark mass is reconstructed up to $m_{\tilde{q}} \sim 1.4 m_{\tilde{g}}$ when $m_{\tilde{g}} \sim 1.4\,\mathrm{TeV}$.

There have been different approaches to mass determination in LHC physics studies. One of the directions is to study inclusive quantities such as $M_{\rm eff}$ or $E_T^{\rm miss}$, which do not require reconstruction and are useful for grabbing the character of the events. The other direction is to study quantities which are specific to some processes such as the end point measurements of the invariant mass and m_{T2} distributions. They are very powerful in determining absolute sparticle masses. In this paper, we propose an inclusive m_{T2} variable, which is inclusive in the sense that we do not specify the decay channel. However, it has the merit of an exclusive analysis with the help of a new understanding of the stransverse mass function $m_{T2}(m_\chi)$. While detailed analyses on the systematical uncertainties are still needed, we hope that this quantity will help to determine sparticle masses.

Acknowledgments

This work is supported in part by the Grant-in-Aid for Science Research, Ministry of Education, Culture, Sports, Science and Technology, Japan (No.16081207, 18340060 for M.M.N. and No. 16081208, 19204027 for K.K). We would like to thank Matt Buckley for a careful reading of this manuscript.

References

[1] H.P. Nilles, *Supersymmetry, supergravity and particle physics*, *Phys. Rept.* **110** (1984) 1.

[2] H.E. Haber and G.L. Kane, *The search for supersymmetry: probing physics beyond the standard model*, *Phys. Rept.* **117** (1985) 75.

[3] S.P. Martin, *A supersymmetry primer*, hep-ph/9709356.

[4] H.-C. Cheng and I. Low, *TeV symmetry and the little hierarchy problem*, *JHEP* **09** (2003) 051 [hep-ph/0308199].

[5] H.-C. Cheng and I. Low, *Little hierarchy, little Higgses and a little symmetry*, *JHEP* **08** (2004) 061 [hep-ph/0405243].

[6] T. Appelquist, H.-C. Cheng and B.A. Dobrescu, *Bounds on universal extra dimensions*, *Phys. Rev.* **D 64** (2001) 035002 [hep-ph/0012100].

[7] CMS collaboration, S. Abdullin et al., *Discovery potential for supersymmetry in CMS*, *J. Phys.* **G 28** (2002) 469 [hep-ph/9806366].

[8] ATLAS collaboration, *ATLAS detector and physic perrformance Technical Design Report*, CERN-LHCC-99-14, CERN-LHCC-99-15 (1999).

[9] I. Hinchliffe, F.E. Paige, M.D. Shapiro, J. Soderqvist and W. Yao, *Precision SUSY measurements at LHC*, *Phys. Rev.* **D 55** (1997) 5520 [hep-ph/9610544].

[10] I. Hinchliffe and F.E. Paige, *Measurements in SUGRA models with large* $\tan\beta$ *at LHC*, *Phys. Rev.* **D 61** (2000) 095011 [hep-ph/9907519].

[11] H. Bachacou, I. Hinchliffe and F.E. Paige, *Measurements of masses in SUGRA models at LHC*, *Phys. Rev.* **D 62** (2000) 015009 [hep-ph/9907518].

[12] B.C. Allanach, C.G. Lester, M.A. Parker and B.R. Webber, *Measuring sparticle masses in non-universal string inspired models at the LHC*, *JHEP* **09** (2000) 004 [hep-ph/0007009].

[13] C.G. Lester and D.J. Summers, *Measuring masses of semi-invisibly decaying particles pair produced at hadron colliders*, *Phys. Lett.* **B 463** (1999) 99 [hep-ph/9906349].

[14] A. Barr, C. Lester and P. Stephens, *m_{T2}: the truth behind the glamour*, *J. Phys.* **G 29** (2003) 2343 [hep-ph/0304226].

[15] W.S. Cho, K. Choi, Y.G. Kim and C.B. Park, *Gluino stransverse mass*, *Phys. Rev. Lett.* **100** (2008) 171801 [arXiv:0709.0288].

[16] B. Gripaios, *Transverse observables and mass determination at hadron colliders*, *JHEP* **02** (2008) 053 [arXiv:0709.2740].

[17] A.J. Barr, B. Gripaios and C.G. Lester, *Weighing Wimps with kinks at colliders: invisible particle mass measurements from endpoints*, *JHEP* **02** (2008) 014 [arXiv:0711.4008].

[18] W.S. Cho, K. Choi, Y.G. Kim and C.B. Park, *Measuring superparticle masses at hadron collider using the transverse mass kink*, *JHEP* **02** (2008) 035 [arXiv:0711.4526].

[19] F. Moortgat and L. Pape, *CMS Physics TDR*, Vol. II, CERN-LHCC-2006, chapter 13.4, page 410.

[20] S. Matsumoto, M.M. Nojiri and D. Nomura, *Hunting for the top partner in the littlest Higgs model with T-parity at the LHC*, *Phys. Rev.* **D 75** (2007) 055006 [hep-ph/0612249].

[21] C. Lester and A. Barr, *MTGEN : mass scale measurements in pair-production at colliders*, *JHEP* **12** (2007) 102 [arXiv:0708.1028].

[22] K. Choi, A. Falkowski, H.P. Nilles, M. Olechowski and S. Pokorski, *Stability of flux compactifications and the pattern of supersymmetry breaking*, *JHEP* **11** (2004) 076 [hep-th/0411066].

[23] K. Choi, A. Falkowski, H.P. Nilles and M. Olechowski, *Soft supersymmetry breaking in KKLT flux compactification*, *Nucl. Phys.* **B 718** (2005) 113 [hep-th/0503216].

[24] K. Choi, K.S. Jeong and K.-i. Okumura, *Phenomenology of mixed modulus-anomaly mediation in fluxed string compactifications and brane models*, *JHEP* **09** (2005) 039 [hep-ph/0504037].

[25] M. Endo, M. Yamaguchi and K. Yoshioka, *A bottom-up approach to moduli dynamics in heavy gravitino scenario: superpotential, soft terms and sparticle mass spectrum*, *Phys. Rev.* **D 72** (2005) 015004 [hep-ph/0504036].

[26] K. Kawagoe and M.M. Nojiri, *Discovery of supersymmetry with degenerated mass spectrum*, *Phys. Rev.* **D 74** (2006) 115011 [hep-ph/0606104].

[27] F.E. Paige, S.D. Protopopescu, H. Baer and X. Tata, *ISAJET 7.69: a Monte Carlo event generator for pp, $\bar{p}p$ and e^+e^- reactions*, hep-ph/0312045.

[28] G. Corcella et al., *HERWIG 6: an event generator for hadron emission reactions with interfering gluons (including supersymmetric processes)*, *JHEP* **01** (2001) 010 [hep-ph/0011363]; *HERWIG 6.5 release note*, hep-ph/0210213.

[29] E. Richter-Was, *AcerDET: a particle level fast simulation and reconstruction package for phenomenological studies on high p_T physics at LHC*, hep-ph/0207355.

JHEP06(2008)035